14th World Congress on Computational Mechanics (WCCM)
ECCOMAS Congress 2020
Virtual Congress: 11–15 January 2021, Paris, France
F. Chinesta, R. Abgrall, O. Allix and M. Kaliske (Eds)

OPTIMAL PRESSURE BOUNDARY CONTROL OF STEADY MULTISCALE FLUID-STRUCTURE INTERACTION SHELL MODEL DERIVED FROM KOITER EQUATIONS

ANDREA CHIERICI[1], LEONARDO CHIRCO[1], VALENTINA GIOVACCHINI[1], SANDRO MANSERVISI[1] AND EMANUELA MARZI[1]

[1] University of Bologna - DIN
Via dei Colli 16, 40136 Bologna (BO), Italy
e-mail: andrea.chierici4@unibo.it

Key words: Optimal Boundary Control, Adjoint Variables, Multiscale FSI

Abstract. The fluid-structure interaction (FSI) problem has been extensively studied, and many papers and books are available in the literature on the subject. In this work, we consider some optimal FSI pressure boundary control applications by using a membrane model derived from the Koiter shell equations where the thickness of the solid wall can be neglected and the computational cost of the numerical problem reduced. We study the inverse problem with the aim of achieving a certain objective by changing some design parameters (e.g. forces, boundary conditions or geometrical domain shapes) by using an optimal control approach based on Lagrange multipliers and adjoint variables. In particular, a pressure boundary optimal control is presented in this work. The optimality system is derived from the first-order optimality condition by taking the Fréchet derivatives of the Lagrangian with respect to all the variables involved. This system is solved by using a finite element code with mesh-moving capabilities. In order to support the proposed approach, we perform numerical tests where the pressure on a fluid domain boundary controls the displacement that occurs in a well-defined region of the solid domain.

1 Introduction

Recently, the numerical simulations of fluid-structure interaction (FSI) problems have become more and more popular, and many papers and books have been published on this topic (see [1, 2, 3, 4, 5]). The applications of the numerical modeling of FSI systems are various, raging from wind turbines and aircraft to hemodynamics. In FSI problems the fluid flow changes the tensional state of a solid structure that is left free to move and the solid deformation has an important effect on the fluid flow.

Several techniques have been developed to reduce the computational cost of FSI problems. In this respect, this work is based on the reduction of the dimensionality of the solid, through a model built on the Koiter shell equations [6]. In order to couple the fluid and the structure domains, the Koiter shell equations are embedded into the fluid equations as a Robin boundary condition [7]. The coupling fluid-structure conditions are automatically treated implicitly, so the stability of this numerical scheme is preserved. This model has many applications in cases where a fluid interacts with a thin membrane that deforms mainly in the normal direction.

In the last years optimization problems have gained popularity among the research community by using gradient-based adjoint methods, see [8, 9]. For adjoint FSI optimization the interested reader can see [10, 11, 12, 13] and the references therein. In this paper, we solve a stationary displacement matching problem where the control variable is the fluid boundary pressure using the Lagrangian multipliers method to obtain the optimality system. The rest of this paper is organized as follows. In Section 2 we introduce the mathematical model describing our multi-scale FSI problem and in Section 3 we derive the optimality system arising from the minimization of the augmented Lagrangian is presented. In Section 4 some simple two-dimensional numerical results are then reported.

2 Physical model

In this section we introduce the mathematical model for the FSI problem. We consider the classic Navier-Stokes equations to model the fluid motion, and a shell model to describe the solid behavior. In particular, the structural model is based on the Koiter shell approach that considers the model of an elastic thin membrane. We introduce now some functional spaces defined on the domain Ω used in the rest of the paper: we denote with $L^2(\Omega)$ the space of square integrable functions, and with $H^s(\Omega)$ the standard Sobolev space with norm $\|\cdot\|_s$. Moreover, we denote with $H_0^s(\Omega)$ the space of all functions in $H^s(\Omega)$ that vanish on the boundary of Ω.

The Koiter shell approach relies on the assumptions that the structure displacements are small and normal to the shell surface. The domain of the structure is denoted by Γ_s, the displacement and the external surface force vectors by $\boldsymbol{\eta}$ and $\mathbf{f_s}$, respectively [7, 14]. The weak form of the considered shell equation results

$$\int_{\Gamma_s} \rho_s h_s \frac{\partial^2 \boldsymbol{\eta}}{\partial t^2} \cdot \boldsymbol{\psi}\, d\Gamma + \int_{\Gamma_s} h_s E^{\alpha\beta\lambda\delta} \gamma_{\alpha\beta}(\boldsymbol{\eta}) \gamma_{\lambda\delta}(\boldsymbol{\psi})\, d\Gamma = \int_{\Gamma_s} \mathbf{f}_s \cdot \boldsymbol{\psi}\, d\Gamma\,, \tag{1}$$

for appropriate test functions $\boldsymbol{\psi}$ belonging to a functional space to be determined on the basis of the imposed boundary conditions. Furthermore, ρ_s and h_s are the density and the thickness of the shell, and $E^{\alpha\beta\lambda\delta}$ and $\gamma_{\alpha\beta}$ are the elasticity and the change of metric, respectively.

In this work negligible bend, shear stresses, and linear elastic constitutive law with a homogeneous and isotropic material are considered [6]. Under these hypotheses the structure model (1) reduces to a simple scalar equation. The dimension of the structure is then reduced by one. So the following simplified model is obtained

$$\begin{aligned} &\rho_s h_s \frac{\partial^2 \boldsymbol{\eta}_3}{\partial t^2} + \beta \boldsymbol{\eta}_3 = f_s && \text{on} \quad \Gamma_s\,, \\ &\boldsymbol{\eta}_3|_{t=0} = \boldsymbol{\eta}_0\,, \qquad \left.\frac{\partial \boldsymbol{\eta}_3}{\partial t}\right|_{t=0} = \boldsymbol{\eta}_v && \text{on} \quad \Gamma_s\,, \end{aligned} \tag{2}$$

where ρ_f and $\mathbf{u}$ are the density and the velocity vector of the fluid, respectively, and $\boldsymbol{\eta}_3$ represents the displacement normal to the reference solid surface. In particular, when one considers cylindrical geometries of radius R, it can be demonstrated that [7]

$$\beta = \frac{h_s E}{1-\nu^2} \frac{1}{R^2}\,, \tag{3}$$

The fluid is modeled as Newtonian, homogeneous and incompressible, described in ALE form as [2, 15]

$$\rho_f \frac{\partial \mathbf{u}}{\partial t}\bigg|_{\mathcal{A}} + \rho_f[(\mathbf{u}-\mathbf{w})\cdot\nabla]\mathbf{u} - \nabla\cdot\boldsymbol{\sigma}^f = \mathbf{0} \quad \text{on} \quad \Omega_f \,, \tag{4}$$

where ρ_f and $\mathbf{u}$ are the density and the velocity vector of the fluid. Moreover, $\boldsymbol{\sigma}^f$ is the Cauchy stress tensor of the fluid written as $\boldsymbol{\sigma}^f = -p\mathbf{I} + \mu(\nabla\mathbf{u} + \nabla\mathbf{u}^T)$, μ and p are the dynamic viscosity and the pressure of the fluid, respectively. The system of equations (4) is completed with appropriate boundary conditions. The fluid domain is Ω_f, and $\mathbf{w}$ is the ALE velocity that determines step by step the position of the nodes of the fluid domain as $\mathbf{x}_f(t) = \mathbf{x}_0 + \int_0^t \mathbf{w} d\tau$.

This shell model allows us to reduce by one the dimension of the solid, so the structural equations can be reduced to a boundary condition on Γ_s for the fluid problem. The two sub-systems (4) and (2) can be coupled by imposing $\boldsymbol{\sigma}^f \cdot \mathbf{n} - f_s = 0$ on Γ_s. We define now the functional space $V^0 = \{\boldsymbol{\phi} \in H^1(\Omega_f) : \boldsymbol{\phi}|_{\Gamma_{D,f}} = \mathbf{0}\}$, where $\Gamma_{D,f}$ are the boundaries of Ω_f where a Dirichlet condition is imposed. In order to satisfy the continuity of the test functions $\boldsymbol{\phi}\cdot\mathbf{n} = \psi$ over the interface surface Γ_s in the coupled system, we introduce the following functional space

$$W^0 = \{(\boldsymbol{\phi}, \psi) \in V^0 \times H^1(\Gamma_s) : \ \boldsymbol{\phi}\cdot\mathbf{n} = \psi \ \text{ over } \Gamma_s\} \,. \tag{5}$$

Now we can derive the weak form of the coupled final system

$$\begin{aligned} &\rho_f\Big(\frac{\partial \mathbf{u}}{\partial t}\bigg|_{\mathcal{A}}, \ \boldsymbol{\phi}\Big) + \rho_f\Big([(\mathbf{u}-\mathbf{w})\cdot\nabla]\mathbf{u}, \ \boldsymbol{\phi}\Big) + \int_{\Omega_f} \boldsymbol{\sigma}^f : \nabla\boldsymbol{\phi} \, d\mathbf{x} - \int_{\Gamma_{N,t}} \mathbf{h}\cdot\boldsymbol{\phi} \, d\Gamma \\ &\qquad + \int_{\Gamma_s} \rho_s h_s \frac{\partial^2 \boldsymbol{\eta}}{\partial t^2}\,\psi \, d\Gamma \ + \int_{\Gamma_s} \beta\boldsymbol{\eta}\psi \, d\Gamma = 0 \,, \\ &(\nabla\cdot\mathbf{u}, \ q) = 0 \,, \end{aligned} \tag{6}$$

for all $(\boldsymbol{\phi}, \psi) \in W^0$, $q \in L^2(\Omega_f)$. A finite element technique is used to obtain the discrete weak formulation of (6). Following the work in [7], we treat explicitly the position of the fluid domain, and consider an implicit discretization of the coupling conditions. With this approach, the structural equation can be incorporated into the fluid equations as a boundary condition (Robin scheme).

However, this work is based on the stationary solution of the presented system. Under this hypothesis, the system (6) becomes

$$\begin{aligned} &\rho_f\Big((\mathbf{u}\cdot\nabla)\mathbf{u}, \ \boldsymbol{\phi}\Big) + \int_{\Omega_f} \boldsymbol{\sigma}^f : \nabla\boldsymbol{\phi} \, d\mathbf{x} - \int_{\Gamma_{N,t}} \mathbf{h}\cdot\boldsymbol{\phi} \, d\Gamma + \int_{\Gamma_s} \beta\boldsymbol{\eta}\psi \, d\Gamma = 0 \,, \\ &(\nabla\cdot\mathbf{u}, \ q) = 0 \,. \end{aligned} \tag{7}$$

3 Optimality system

In this work, we are interested in solving a given shell deformation by controlling the fluid pressure over a boundary. For this purpose, we start introducing the following objective functional

$$\mathcal{J}(\boldsymbol{\eta}, p) = \frac{1}{2}\int_{\Gamma_d} \|\boldsymbol{\eta} - \boldsymbol{\eta}_d\|^2 \, d\Gamma + \frac{\lambda}{2}\int_{\Gamma_c} p^2 \, d\Gamma \,, \tag{8}$$

where the first term is the distance in norm between the actual displacement and the desired value over the controlled boundary Γ_d, and the second term is a standard Tychonov regularization term that limits the L^2-norm of the fluid boundary pressure p_c, i.e. the control variable. The regularization parameter λ weights the importance of the two terms over the cost functional. In general, too much regularization leads to smoother but less effective controls, while a lack of regularization may cause numerical issues since usually the optimal solution lies in distributional spaces.

We now introduce the following augmented Lagrangian functional $\mathcal{L}$, that is obtained by adding to the objective functional $\mathcal{J}$ the FSI state equations (7) multiplied by a set of Lagrange multipliers. In the following, we refer to the Lagrange multipliers as *adjoint variables*.

$$\begin{aligned}\mathcal{L}(\boldsymbol{\eta}, \mathbf{u}, \mathbf{u}_a, p, p_a, \Gamma) = \mathcal{J}(\boldsymbol{\eta}, p) - (\rho^f(\mathbf{u}\cdot\nabla)\mathbf{u},\ \mathbf{u}_a) + (p,\ \nabla\cdot\mathbf{u}_a) - (p_a,\ \nabla\cdot\mathbf{u}) \\ - \mu(\nabla\mathbf{u},\ \nabla\mathbf{u}_a) + \int_\Gamma \mu(\nabla\mathbf{u}\cdot\mathbf{n})\cdot\mathbf{u}_a d\Gamma - \int_\Gamma (p\mathbf{n})\cdot\mathbf{u}_a d\Gamma - \int_{\Gamma_t} \mathbf{u}_a\cdot(\beta\boldsymbol{\eta} - \mathbf{f}_s - \boldsymbol{\tau}_n) d\Gamma\,,\end{aligned} \tag{9}$$

where we integrate by parts the contributions of the fluid stress tensor $\boldsymbol{\sigma}^f$. The surface integrals can be rewritten by substituting the definition of $\boldsymbol{\tau}_n$. The stationary points of the Lagrangian functional can be found by setting to zero the Fréchet derivatives taken for all the problem variables. When the derivatives are taken with respect to the adjoint variables the weak form of the state system (7) is recovered as well as the boundary conditions. By taking the derivatives in the direction δp we get

$$\frac{D\mathcal{L}}{Dp}\delta p = (\nabla\cdot\mathbf{u}_a,\ \delta p) - \int_{\Gamma-\Gamma_t} (\mathbf{u}_a\cdot\mathbf{n})\delta p\, d\Gamma + + \int_{\Gamma_c} \lambda p\,\delta p\, d\Gamma = 0 \quad \forall \delta p \in L^2(\Omega)\,. \tag{10}$$

By considering the volume integral we get the following continuity equation for the adjoint velocity

$$\nabla\cdot\mathbf{u}_a = 0 \qquad \text{on } \Omega\,, \tag{11}$$

while, with the surface contributions, we recover the *control equation* over the controlled boundary Γ_c

$$\int_{\Gamma-\Gamma_t} (\mathbf{u}_a\cdot\mathbf{n})\delta p\, d\Gamma - \int_{\Gamma_c} \lambda p\,\delta p\, d\Gamma = 0 \quad \forall \delta p \in L^2(\Omega) \quad \Rightarrow \quad p = \frac{\mathbf{u}_a\cdot\mathbf{n}}{\lambda} \qquad \text{on } \Gamma_c\,, \tag{12}$$

and the boundary conditions on Γ_D

$$\int_{\Gamma-\Gamma_t-\Gamma_c} (\mathbf{u}_a\cdot\mathbf{n})\delta p\, d\Gamma = 0 \quad \forall \delta p \in L^2(\Omega) \quad \Rightarrow \quad \mathbf{u}_a\cdot\mathbf{n} = 0 \qquad \text{on } \Gamma_D\,, \tag{13}$$

On Γ_N we have $\delta p = 0$ since we prescribe Neumann boundary conditions with fixed pressure.

For $\delta\boldsymbol{\eta}$ we have

$$\frac{D\mathcal{L}}{D\boldsymbol{\eta}}\delta\boldsymbol{\eta} = -\int_{\Gamma_t} \mathbf{u}_a\cdot\beta\,\delta\boldsymbol{\eta} d\Gamma + \int_{\Gamma_d} (\boldsymbol{\eta} - \boldsymbol{\eta}_d)\cdot\delta\boldsymbol{\eta} d\Gamma = 0 \quad \forall \delta\boldsymbol{\eta} \in W^0\,. \tag{14}$$

Recalling that $\Gamma_d \subset \Gamma_t$ we obtain the following boundary conditions for the adjoint system

$$\begin{aligned}\mathbf{u}_a\beta - (\boldsymbol{\eta} - \boldsymbol{\eta}_d) = 0 \qquad &\text{on } \Gamma_d\,, \\ \mathbf{u}_a\beta = 0 \qquad &\text{on } \Gamma_t\,.\end{aligned} \tag{15}$$

We collect $\delta\mathbf{u}$ terms and integrate by parts to obtain

$$\begin{aligned}\rho^f([(\delta\mathbf{u}\cdot\nabla)\mathbf{u}+(\mathbf{u}\cdot\nabla)\delta\mathbf{u}]\,,\ \mathbf{u}_a)-(\nabla p_a,\ \delta\mathbf{u})-\mu(\nabla^2\mathbf{u}_a,\ \delta\mathbf{u})+\int_\Gamma(p_a\mathbf{n})\cdot\delta\mathbf{u}\,d\Gamma\\ -\int_{\Gamma-\Gamma_t}\mu(\nabla\delta\mathbf{u}\cdot\mathbf{n})\cdot\mathbf{u}_a\,d\Gamma+\int_\Gamma\mu(\nabla\mathbf{u}_a\cdot\mathbf{n})\cdot\delta\mathbf{u}\,d\Gamma=0\quad\forall\delta\mathbf{u}\in W^0\,.\end{aligned}\tag{16}$$

The strong form of the adjoint velocity reads

$$\rho^f(\nabla\mathbf{u})^T\cdot\mathbf{u}_a+\rho^f(\mathbf{u}\cdot\nabla)\mathbf{u}_a-\nabla p_a-\mu\nabla^2\mathbf{u}_a=0\qquad\text{on }\Omega\,,\tag{17}$$

with boundary conditions

$$\mathbf{u}_a\ =0\quad\text{on }\Gamma_D,\qquad\boldsymbol{\tau}_{na}=0\quad\text{on }\Gamma_N\cup\Gamma_t\,.\tag{18}$$

Moreover we have to consider the contribution on $\mathcal{L}$ given by the motion of the boundary Γ_t along the direction $\delta\boldsymbol{\eta}$

$$\frac{D\mathcal{L}}{D\Gamma}\delta\boldsymbol{\eta}=\int_{\Gamma_t}\beta(\nabla\mathbf{u}_a\cdot\mathbf{n}+\chi\mathbf{u}_a)\cdot\delta\boldsymbol{\eta}\,d\Gamma=0\quad\forall\delta\boldsymbol{\eta}\in W^0\,,\tag{19}$$

where χ represents the shell curvature. Under the hypothesis of small deformation we can safely neglect the terms where χ appears. We also have that $\frac{D\mathcal{L}}{D\Gamma}\delta\boldsymbol{\eta}=0$ since the term with $\mathbf{u}_a$ is defined on the surface Γ_t, and a constant extension of it towards the normal direction to the surface leads to a null normal gradient of this term.

In short the optimality system consists of the state system (7), the control equation (12), the adjoint system (11)-(16) and the boundary conditions (13)-(15)-(18). Since the optimality system doubles the state variables the use of a *one-shot* method is not appropriate and we use a segregated approach for the solution of the state, adjoint, and gradient equations. An advantage of our monolithic aproach is that we can reuse the same solver for both the solution of the state (7) and adjoint systems (11)-(16) with few modifications.

4 Numerical results

In this section, we report some numerical results obtained by using the mathematical model shown in the previous sections. We consider a rectangular domain $\Omega=\{(x,y):x\in[0,0.1],y\in[0,0.3]\}$ as shown in Figure 1 on the left. The fluid has density $\rho^f=1000\ kg/m^3$ and dynamic viscosity $\mu=100\ Pa\cdot s$. For the solid, we consider $\beta=60kPa/m$ and thickness $h_s=0.0075\ m$. For all the presented simulations, the domain was uniformly divided with a regular rectangular mesh.

We implement a standard steepest descent algorithm in the multigrid finite element code FEMuS, that relies on PETSc libraries for the solution of the multigrid discretized linear solver with MPI paralellization.

4.1 Plane channel test

In this first test, the fluid flows vertically from the bottom to the top. The region of the boundary Γ_2 represents a solid wall with no-slip boundary condition ($\mathbf{u}=\mathbf{0}$) and Γ_3 is the membrane where we

impose the generalized Robin boundary condition (2). In Figure 1, we also report the results obtained simulating the system without control and in steady-state. The displacement of the points in the domain (center) and the pressure (right) are shown. The pressure presents a linearly decreasing trend from the bottom, where $p = 6000\ Pa$ is imposed, to the top, where we fixed $p = 0\ Pa$, and it is shown with lines of iso-magnitude.

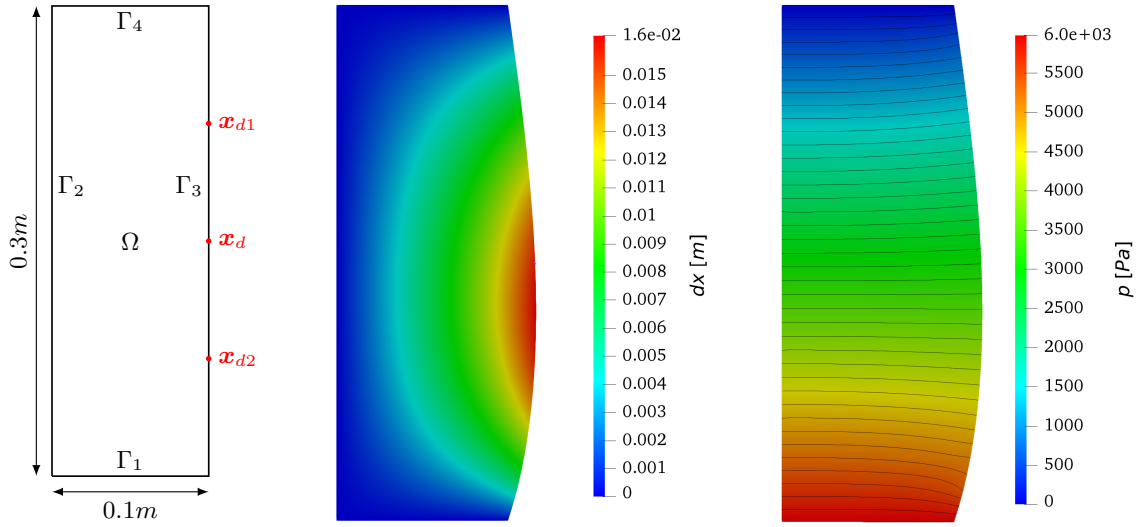

Figure 1: Geometry and controlled region used in the plane channel (with $\Omega_d = \mathbf{x_d}$) and airbag (with $\Omega_d = \mathbf{x_{d1}} \cup \mathbf{x_{d2}}$) tests (left). Deformation η (center) and pressure p (right) in Ω in steady state without control.

The simulations aim to control the displacement of the point $\mathbf{x_d}$ of the membrane, along the x-direction, optimizing the pressure of the fluid on Γ_1. This point, without control, shows a displacement $\eta = 0.015824\ m$. The objective of the optimization is to reduce η_d to $0.005\ m$, changing the pressure of the fluid on Γ_1. The objective functional of the problem reads

$$\mathcal{J}(\eta, p) = \frac{1}{2}(\eta|_{\mathbf{x_d}} - \eta_d)^2 + \frac{\lambda}{2}\int_{\Gamma_1} p^2\, d\Gamma\,. \tag{20}$$

We solve multiple simulations with different regularization parameter λ. The results are presented in Table 1. Note that the smaller is λ, the closer the displacement of the controlled point $\mathbf{x_d}$ is to the desired one. This result is expected, since with larger λ the contribution of the regularization term in the minimization of the functional is more relevant. This is introduced in the functional in order to limit the control parameter p to the space of square integrable functions. Therefore, with larger λ we find more regular optimization parameter p, but less precise displacement field η. In Table, we also report the number of iterations needed for the implemented algorithm to find the optimal solution.

We focus now on the controlled inlet pressure field updated through the formula

$$p_c^i = p_c^{i-1} - r^{i,j}\left(p_c^{i-1} - \frac{\mathbf{u}_a^i \cdot \mathbf{n}}{\lambda}\right)\,. \tag{21}$$

Table 1: Objective functional $\mathcal{J}$, displacement η and number of iteration obtained with different λ values.

λ	$\mathcal{J}(\eta, p_c)$	$\eta_{opt}[m]$	Iterations
∞	$5.85839 \cdot 10^{-05}$	0.015824	–
10^{-08}	$2.19246 \cdot 10^{-06}$	0.002906	4
10^{-09}	$5.54438 \cdot 10^{-09}$	0.004895	8
10^{-10}	$2.18941 \cdot 10^{-10}$	0.004979	10
10^{-11}	$6.10506 \cdot 10^{-12}$	0.004997	12
10^{-12}	$3.86734 \cdot 10^{-15}$	0.005000	26

In fact, depending on the regularization parameter, different inlet pressure fields can be obtained. In Figure 2, the controlled pressure field along the boundary Γ_1 is reported for various values of λ. Note that the choice of the regularization parameter strongly affects the controlled pressure field. With weak regularization, the objective term dominates in the functional and the pressure attains large values, thus effectively controlling the membrane displacement. In Figure 2 it is also reported the reference starting pressure. The comparison between the uncontrolled field and all the controlled pressure fields show that the control strongly affects the solution on $\Gamma_c = \Gamma_1$ in order to obtain the desired displacement η_d. Moreover, in Figure 2 on the right the velocity field for $\lambda = 10^{-15}$ is reported. Note that an inversion of the fluid flow in the inlet occurs, needed for reducing the displacement of the point $\mathbf{x_d}$.

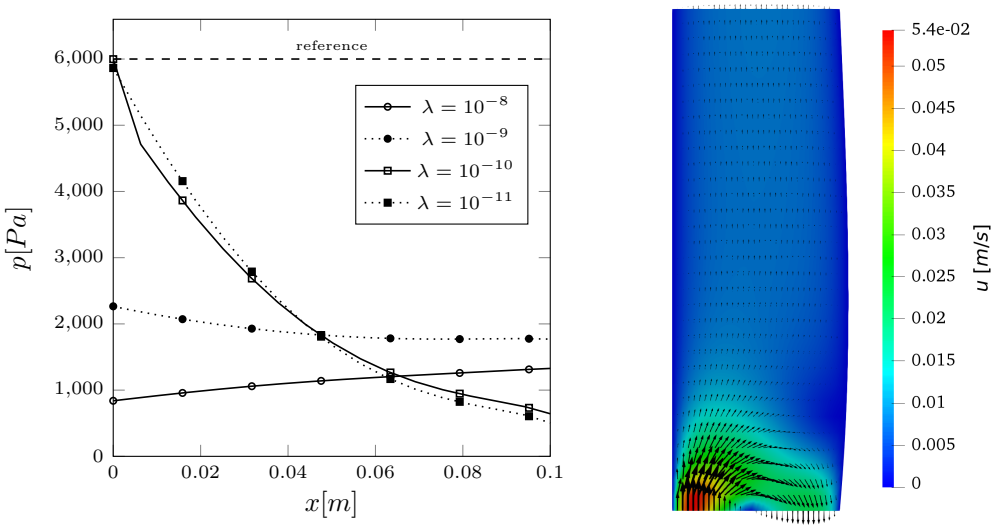

Figure 2: Plane channel test: control pressure p on Γ_1 with different regularization parameters (left). The dotted line represents the pressure in the reference case with no control (i.e. $\lambda = \infty$). On the right: velocity $\mathbf{u}$ in Ω for $\lambda = 10^{-15}$.

4.2 Airbag test

We consider the same geometry of the previous test, togheter with airbag-like boundary conditions: we impose a no-slip condition on $\Gamma_1 \cup \Gamma_4$ and the Koiter boundary condition on Γ_3. The controlled pressure is imposed on $\Gamma_c = \Gamma_2$, where we initially impose $p = 300\ Pa$. We also consider all the physical properties introduced above. In this framework we want to control the displacement field on the two different points, $\boldsymbol{x}_{d1}$ and $\boldsymbol{x}_{d2}$ (see Figure 1, left).

Observing the results obtained in a steady state without control, shown in Figure 3, one can see that the problem is symmetric since we are neglecting the buoyancy forces. The two points $\mathbf{x_{d_1}}$ and $\mathbf{x_{d_2}}$ present a displacement $\eta = 0.001152\ m$ and the pressure in the channel is almost constant everywhere.

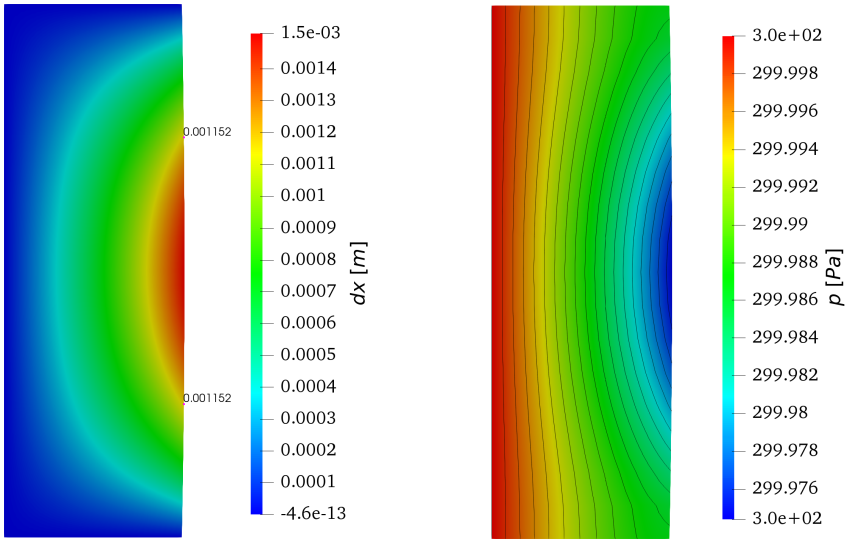

Figure 3: Airbag test: behavior of the displacement η (center) and the pressure p (right) in the reference case with no control. The points $\boldsymbol{x}_{d1}$ and $\boldsymbol{x}_{d2}$ are highlighted.

The goal is to control the displacement of the two points $\mathbf{x_{d_1}}$ and $\mathbf{x_{d_2}}$, optimizing the pressure of the fluid on the boundary Γ_2. In order to break the symmetry of the problem, we choose a desired displacement of point $\mathbf{x_{d_1}}$ equal to $\eta_{d_1} = -0.01\ m$ and a desired displacement of $\mathbf{x_{d_2}}$ equal to $\eta_{d_2} = 0.01\ m$. The functional associated with the presented numerical problem reads

$$\mathcal{J}(\eta, p_c) = \frac{1}{2}(\eta|_{\mathbf{x_{d_1}}} - \eta_{d_1})^2 + \frac{1}{2}(\eta|_{\mathbf{x_{d_1}}} - \eta_{d_2})^2 + \frac{\lambda}{2}\int_{\Gamma_2} p_c^2\, d\Gamma\,. \tag{22}$$

Many simulations have been done for different regularization parameter λ. In Figure 4, the control parameter p obtained with different values of λ is reported. Note that the trend obtained with $\lambda = 10^{-10}$ shows slightly different values compared to the other two reported cases.

The reason of that is explained in Table 2, where the values of the functional $\mathcal{J}$ and of the displacements on $\mathbf{x_{d_1}}$ and $\mathbf{x_{d_2}}$ are reported for all the inspected λ values. In fact, we can observe that the displacements obtained with $\lambda = 10^{-8}$ and $\lambda = 10^{-12}$ are similar and we are achieving the objective displacement

Table 2: Objective functional $\mathcal{J}$, displacement η and number of iteration obtained with different values of λ.

λ	$\mathcal{J}(\eta, p_c)$	$\eta_{1opt}[m]$	$\eta_{2opt}[m]$	Iterations
∞	$1.01327 \cdot 10^{-4}$	0.001152	0.001152	–
10^{-8}	$2.21289 \cdot 10^{-5}$	-0.010695	0.005348	4
10^{-10}	$1.39504 \cdot 10^{-5}$	-0.011603	0.013374	6
10^{-12}	$2.54909 \cdot 10^{-5}$	-0.010032	0.004951	4

η_{d_2} from a lower value of it. On the contrary, if we consider the results obtained with $\lambda = 10^{-10}$, we see that we are getting to the objective from a larger displacement. In fact, the functional has a different local minimum and the algorithm in this case moved to a different one. In Figure 4, we also reported the

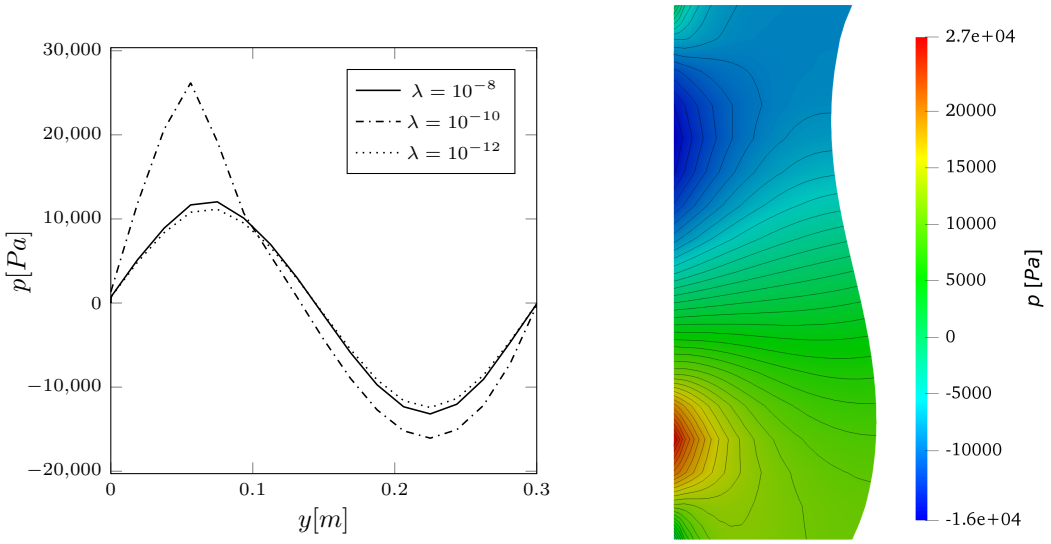

Figure 4: Pressure p on $\Gamma_2 = \Gamma_c$ with different values of λ (left) and pressure p in Ω with $\lambda = 10^{-10}$ (right).

pressure of the fluid in Ω for $\lambda = 10^{-10}$. Again, note that the value of λ affects the pressure field to be imposed on the control domain Γ_2. In this case, the resulting velocity implies an inlet of fluid from a region of Γ_2 close to the point $\mathbf{x_{d_2}}$ of which we want to increase the displacement, and an outlet of the fluid in a region of Γ_2 close to the point $\mathbf{x_{d_1}}$, of which we want to reduce the displacement. In general, this case is an ill-posed control problem, due to various local minima close to each other.

Conclusions

In this work a mathematical and numerical method have been proposed to solve an optimal boundary control problem applied to a fluid-structure interaction model based on the Koiter's equation. Using this formulation, the equations for the solid become boundary conditions for the fluid equations reducing the computational cost of the numerical simulation. Then, we have obtained the optimality system applied to the pressure boundary control problem applied to the introduced Koiter FSI model to find the required

memebrane displacement. We have introduced the steepest descent algorithm and solved the proposed control problem with a finite element code. Some simple numerical results have been presented to show the robustness of the multi-scale mathematical model.

REFERENCES

[1] Turek S and Hron J 2006 *Lecture notes in computational science and engineering* **53** 371

[2] Formaggia L, Quarteroni A and Veneziani A 2010 *Cardiovascular Mathematics: Modeling and simulation of the circulatory system* vol 1 (Springer Science & Business Media)

[3] Bazilevs Y, Takizawa K and Tezduyar T E 2013 *Computational fluid-structure interaction: methods and applications* (John Wiley & Sons)

[4] Le Tallec P and Mouro J 2001 *Computer methods in applied mechanics and engineering* **190** 3039–3067

[5] Cerroni D and Manservisi S 2016 *Journal of Computational Physics* **313** 13–30

[6] Koiter W 1970 *Proc. Int. Congr. of Mathematics, Nice* vol 3 pp 123–130

[7] Nobile F and Vergara C 2008 *SIAM Journal on Scientific Computing* **30** 731–763

[8] Gunzburger M D 2003 *Perspectives in flow control and optimization* vol 5 (Siam)

[9] Gunzburger M D and Manservisi S 2000 *SIAM Journal on Numerical Analysis* **37** 1481–1512

[10] Chirco L and Manservisi S 2019 *Computers & Fluids* **182** 118–127

[11] Richter T and Wick T 2013 *SIAM Journal on Scientific Computing* **35** B1085–B1104

[12] Perego M, Veneziani A and Vergara C 2011 *SIAM J. Scientific Computing* **33** 1181–1211

[13] Chierici A, Chirco L, Da Viá R, Maccari P and Manservisi S 2020 pp 3292–3303

[14] Chierici A, Chirco L, Giovacchini V, Manservisi S and Santesarti G 2020 *Journal of Physics: Conference Series* vol 1599 (IOP Publishing) p 012040

[15] Hughes T J, Liu W K and Zimmermann T K 1981 *Computer methods in applied mechanics and engineering* **29** 329–349